Structural modulation and hole distribution in $Sr_{14-x}Ca_xCu_{24}O_{41}$

2009 J. Phys.: Condens. Matter 21 215606

(http://iopscience.iop.org/0953-8984/21/21/215606)

J. Phys.: Condens. Matter **21** (2009) 215606 (7pp) doi:10.1088/0953-8984/21/21/215606

Structural modulation and hole distribution in $Sr_{14-x}Ca_xCu_{24}O_{41}$

C Ma[1], H X Yang[1], L J Zeng[1], Y Zhang[1], L L Wang[2], L Chen[2], R Xiong[2], J Shi[2,3] and J Q Li[1,4]

[1] Beijing National Laboratory for Condensed Matter Physics, Institute of Physics, Chinese Academy of Sciences, Beijing 100190, People's Republic of China
[2] Department of Physics, Wuhan University, Wuhan 430072, People's Republic of China
[3] International Center for Materials Physics, Chinese Academy of Science, Shenyang 110016, People's Republic of China

E-mail: Ljq@aphy.iphy.ac.cn (J Q Li)

Received 10 November 2008, in final form 28 February 2009
Published 30 April 2009
Online at stacks.iop.org/JPhysCM/21/215606

Abstract

Structural properties and hole distribution in the spin-ladder compound $Sr_{14-x}Ca_xCu_{24}O_{41}$ have been extensively investigated by transmission electron microscopy (TEM). The complex electron diffraction patterns and high-resolution TEM observations reveal a clear incommensurate structural modulation along the c-axis direction attributable to two mismatched sublattices; this modulation strongly depends on hole distribution in the compounds. The fine structures of the O K and Cu $L_{2,3}$ ionization edges for the $Sr_{14-x}Ca_xCu_{24}O_{41}$ compounds recorded under different conditions indicate that more doped holes reside in the chains than the ladders, and that substituting Ca for Sr atoms results in a charge redistribution between the chains and ladders. Based on the experimental findings, the theoretical results, including the partial density of states and optical conductivity spectra calculated by the density functional theory, are also discussed.

(Some figures in this article are in colour only in the electronic version)

1. Introduction

The antiferromagnetic $S = 1/2$ two-leg ladder system, which has a spin liquid ground state with a spin gap, has been the subject of extensive investigations in past decades, owing to its magnetic peculiarities and superconductivity [1, 2]. Recently, a variety of experimental investigations revealed that the spin-ladder system $Sr_{14-x}Ca_xCu_{24}O_{41}$ could be a new class of superconducting materials with the critical temperature (T_c) up to 12 K under a hydrostatic pressure ranging from 3.5 to 4 GPa for samples at $x = 13.6$ [3]. This kind of compound consists of two different types of copper oxide substructures: the edge sharing CuO_2 chain and the two-leg Cu_2O_3 ladder [4], which are separated by a (Sr, Ca) layer stacking in an alternating fashion along the b crystallographic direction, as shown in figure 1. Due to the lattice misfit and interactions between two sublattices, the crystal structure is notably modulated by an incommensurate ratio of c_L and c_C (where c_L and c_C are the c-axis lattice constants of the chains and ladders, respectively) which has a typical value of about 10/7. It is also noted that the nominal valence of Cu ions is +2.25 independent of Ca content (x). Therefore, $Sr_{14-x}Ca_xCu_{24}O_{41}$ is intrinsically doped with six holes per formula unit as counted from the Cu^{2+} state. Measurements with x-ray absorption spectroscopy (XAS) [5, 6] and optical conductivity [7] indicate that doped holes are mostly located in the chains. An insulating hole crystal phase in which the carriers are localized through many-body interactions was observed at about 200 K for the sample at $x = 0$ [8]. On the other hand, hole spins appearing on oxygen sites are expected to couple with copper spins, producing a nonmagnetic state which is usually referred to as the Zhang–Rice singlet [9]. The spin dimer consisting of two Cu^{2+} ions and a Cu^{3+} ion on a Zhang–Rice singlet site in the CuO_2 chains is recognizable as a dramatic decrease in the magnetic susceptibility below 80 K [10], and a fivefold superstructure in the hole ordered state was observed, in which two dimers are separated by two other Zhang–Rice singlets, as discussed in [11]. It is noted that substitution of isovalent Ca for Sr atoms would result in holes transferring from the chains to ladders without changing the total hole density [6, 7].

[4] Author to whom any correspondence should be addressed.

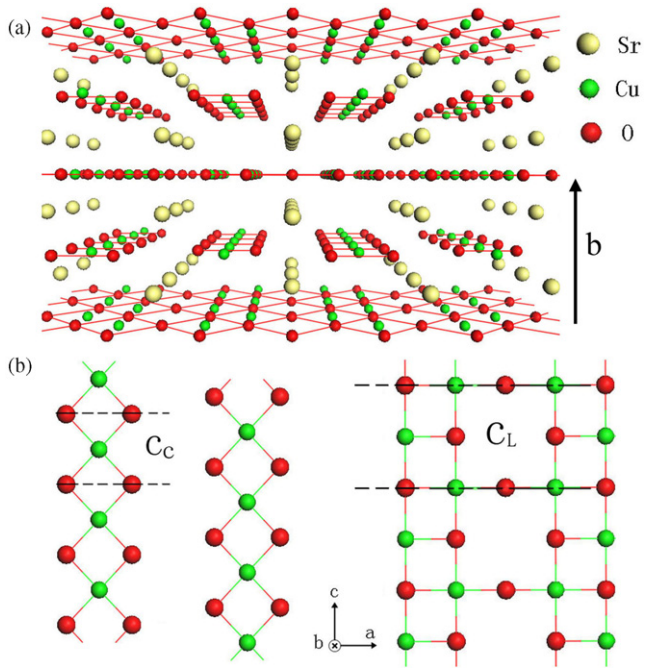

Figure 1. (a) A perspective view of the crystal structure of $Sr_{14-x}Ca_xCu_{24}O_{41}$ along the *c*-axis direction. (b) Structures of two sublattices in the *ac* plane: CuO_2 chains (left) and Cu_2O_3 two-leg ladders (right). The lattice parameters along the *c*-axis direction are c_C and c_L for the chains and ladders, respectively.

However, hole distribution obtained by various measurements is still controversial in the present system. In order to understand the remarkable structural and physical properties of this kind of compound, we should get more knowledge about the hole distribution between the two sublattices and the correlation between the structural modulation and electronic structure.

The well-established transmission electron microscopy (TEM) techniques, including electron diffraction (ED), high-resolution electron microscopy (HREM) and electron energy loss spectroscopy (EELS), allow us to directly reveal microstructure features and the local electronic structure from the same region. Hence, the local electronic alternations associated with a structural transition can be well detected. In this study, we concentrated our attention on the incommensurate structural modulation and hole distribution between the chains and ladders. The ED patterns and HREM images are used to characterize the incommensurate structural modulation, and the electron energy loss (EEL) spectra, collected under different conditions for the well-characterized $Sr_{14-x}Ca_xCu_{24}O_{41}$ samples at $x = 0$ and 5.6, provide rich information about the electronic structure. In addition, we also perform first-principle electronic structure calculations in order to interpret the experimental results better.

2. Experimental details and computational method

The TEM samples used in the present study were prepared by crushing the well-characterized polycrystalline $Sr_{14-x}Ca_xCu_{24}O_{41}$ synthesized by a solid-state reaction [12], and then the resultant suspensions were dispersed on a holey carbon-covered Cu grid. The ED patterns, HREM image and EEL spectra were obtained on a FEI Tecnai-F20 (200 kV) TEM equipped with a Gatan imaging filter (GIF). The energy resolution is about 1.0 eV as measured in each experimental spectrum for the full-width at half-maximum (FWHM) of the zero-loss peak. The EEL spectra were recorded in a conventional TEM diffraction mode with an approximately parallel electron beam. The crystals examined in the experiments were tilted slightly off the zone axes by 1°–2° to avoid the electron channeling effect [13]. The electronic structure calculations were carried out using the full potential linear augmented plane wave (LAPW) method within density functional theory (DFT) via the Wien2k code [14], and we chose the local spin density approximation (LDA) as the exchange–correlation potential. The structural parameters of the chains and ladders were cited from [15]. The muffin-tin radii R_{mt} were selected as 1.90 au for Cu atoms and 1.55 au for O atoms and $R_{mt}K_{max}$ was set to 7.0 to determine the basis size.

3. Results and discussion

Figure 2 shows the ED patterns and HREM image for $Sr_{14}Cu_{24}O_{41}$ taken along the different zone-axis directions. It is notable that the ED patterns in general are complicated due to structural incommensurability and the multiple diffraction effect. Figure 2(a) clearly illustrates all diffraction features from the chains and ladders in which the lattice parameters c_C and c_L are about 2.73 and 3.92 Å, respectively [15]. As shown in this ED pattern, the smaller and larger meshes composed of relatively intense spots arise from systematic diffraction of the chain and ladder sublattices, respectively, while a series of weak satellite spots are produced by multiple diffraction. It should be pointed out that these satellite spots along the c^*-axis direction observed in the $[1\bar{1}0]$ zone-axis ED pattern show visibly different features in comparison with those observed in the [010] zone-axis ED pattern (figure 2(b)). This fact suggests that these satellite spots originate from multiple diffraction rather than intrinsic superstructure, as clearly shown in the inset of figure 2(a), in good agreement with the data reported in [16]. The positions of the satellite spots are fundamentally governed by the lattice misfit of two sublattices, namely, the ratio of c_L and c_C, which in the present case is about 13/9 depending on the calcium and oxygen content, as discussed by Hiroi *et al* [17].

In addition, our *in situ* cooling and heating TEM observations demonstrate that neither new superstructure nor substantial change in the structural modulation is observed between 20 and 600 K, except for a slight increase in the intensities of the satellite spots. These results coincide with the previous observations by electron and x-ray diffractions [17, 18] in which the weak reflections appearing at low temperature are considered to originate from the high-order reflections.

Figure 2(d) shows the HREM image taken along the [130] zone-axis direction at room temperature, showing the apparent modulated stripes along the *c*-axis direction. As shown in the corresponding ED pattern (figure 2(c)), the intense diffraction

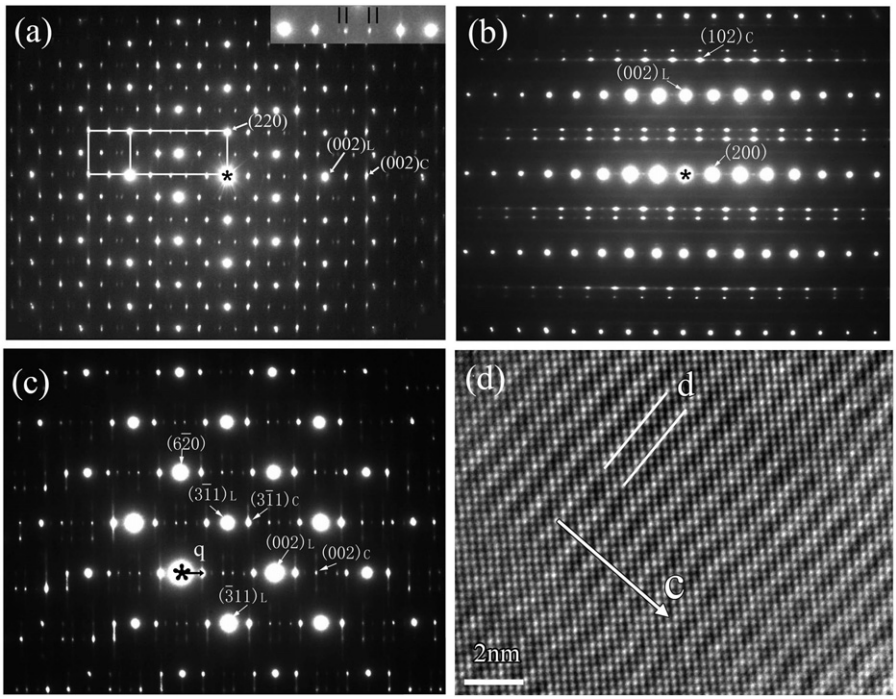

Figure 2. ED patterns of $Sr_{14}Cu_{24}O_{41}$ taken along the [1$\bar{1}$0] (a), [010] (b) and [130] (c) zone-axis directions at room temperature, respectively. The small rectangle with intense spots comes from the ladder sublattice and the large one with weak spots from the chain sublattice. The inset in (a) shows the magnified satellite spots sequence along the c^* direction. The HREM image (d) taken along the [130] zone-axis direction clearly shows the incommensurate modulation.

spots uniquely arise from the ladders. Therefore, this HREM image chiefly reflects the average structural features of the ladders, and the lattice misfit between the chains and ladders only gives rise to modulation in the lattice image. Hence, it is possible to associate the stripes with the parallel Moiré fringe arising from the two interpenetrating structures, and the resultant period, $d = (c_L \cdot c_C)/(c_L - c_C)$, is about 9 Å, corresponding to the vector **q** as indicated in figure 2(c).

Due to weak hybridization between different atomic layers, namely, the CuO_2 chains, Cu_2O_3 ladders and electron donor Sr (Ca) layers [19], it is feasible to treat independently the chains and ladders in theoretical calculations. We performed electronic structure calculations using the LDA method for both the chains and the ladders. The band structure exhibits apparent one-dimensional character along the c-axis direction. Figure 3 shows the projected density of states towards the O 2p orbitals for the chains and ladders. Careful analysis suggests that only σ bonding between Cu(c) $-$ d_{xz} (Cu(l) $d_{x^2-z^2}$) and O $p_x + p_z$ states (where x, y and z point to the a, b and c crystallographic direction, respectively) contributes to spectral weight near the Fermi level (E_F). These features can be revealed quite well by the EELS measurements, as discussed in the following sections. Due to the ligand field effect and strong on-site Coulomb interaction, the Cu 3d states are split into two components, i.e. the lower and upper Hubbard bands, between which are the O 2p states strongly hybridized with the Cu 3d states. For the CuO_2 chains, the density of states shows a charge-transfer gap of about 0.8 eV between the high-lying Cu 3d states and the O 2p states below E_F as observed in most cuprate superconductors. However,

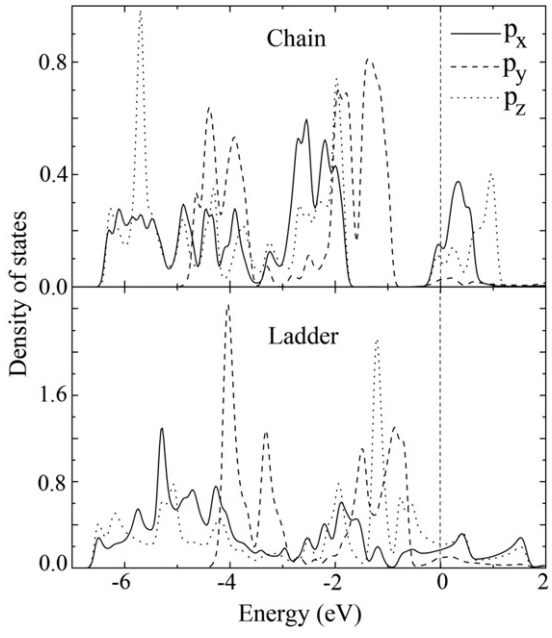

Figure 3. Projected density of states towards the O 2p orbitals for the chain (upper panel) and ladder (lower panel) sublattices calculated independently by the LDA method.

no energy gap is apparent in the Cu_2O_3 ladders, as predicted by the previous calculations [19, 20]. On the other hand, the metallic state of both the chains and ladders obtained by the LDA method contradicts the experimentally observed non-metallic state in the present system. In order to reproduce the

insulating behavior, both electronic correlations and specific charge ordering existing in the present system should be taken into account in calculations.

In order to investigate experimentally the hole states near E_F, we recorded EEL spectra for the O K and Cu $L_{2,3}$ ionization edges (figure 4) in the diffraction mode with the incident electron beam aligned with the *b*-axis. The specific information about the hole states of different orbital character can be obtained through changing the momentum transfer [13]. Here, the momentum transfer can be changed by varying the collection semi-angle. By increasing the collection semi-angle, the spectral weight contributed by the out-of-plane orbitals is steadily transferred to that contributed by the in-plane orbitals, according to the conservation of momentum. As a result, this fact allows us to assign the prepeak at around 529 eV in the O K edge to the in-plane O p_x and p_z states and the peak at around 533 eV to the out-of-plane O p_y states. The intense peaks in the Cu $L_{2,3}$ edges are predominantly contributed by the in-plane Cu(c) d_{xz} and Cu(l) $d_{x^2-z^2}$ orbitals. The most striking feature observed in both the O K and Cu $L_{2,3}$ edges is the presence of two sub-peaks (figure 4) which have been extensively discussed in the high-T_c superconductors [21] in which holes generally have the O 2p character.

According to the charge-transfer model [22], the low-energy peak H at around 528.0 eV in the O K edge arises from the hole states on the O 2p orbitals and the high-energy peak U at around 529.4 eV from the O 2p states which are strongly hybridized with the Cu 3d states on the upper Hubbard band. The energy difference between H and U represents a charge-transfer gap of about 1.4 eV, which is larger than the theoretical one because the LDA calculation usually underestimates the energy gap. As mentioned above, the Cu $L_{2,3}$ edge also exhibits two sub-peaks in both L_2 and L_3 lines. The low-energy peak *a* at around 930.5 eV is assigned to transitions from the $Cu(2p_{3/2})3d^9$ ground states to the $Cu(2p_{3/2})^{-1}3d^{10}$ states (formal bivalent oxidation state) which is considered to be the magnetic Cu ions with $S = 1/2$, where $(2p_{3/2})^{-1}$ denotes the $2p_{3/2}$ hole on Cu ions. The high-energy shoulder *b* at 932.1 eV originates from the O 2p hole states and is assigned to transitions from the $Cu(2p_{3/2})3d^9L$ states to the $Cu(2p_{3/2})^{-1}3d^{10}L$ excited states (formal trivalent oxidation state), where L denotes the O 2p ligand hole. This shoulder, corresponding to the nonmagnetic Cu ions associated with the Zhang–Rice singlet, can provide information about the total concentration of hole states, as discussed in the following section.

Taking into account the difference in lattice parameters between the two sublattices (figure 1), we can distinguish the ladders from the chains in the EEL spectra using the electron channeling effect [23, 24]. The sample is first tilted to make the ladders satisfy the two-beam condition in which only (002) planes are strongly diffracted. Through changing the sign of the deviation parameter **s**, we can maximize the incident-wave intensity on the ladders at negative **s** (case I) or on the chains at positive **s** (case II), as illustrated in figure 5(a). As a result, we have indeed obtained the selectively enhanced spectra for each sublattice. It is noted here that the difference in the O K edges is relatively small because of delocalization of

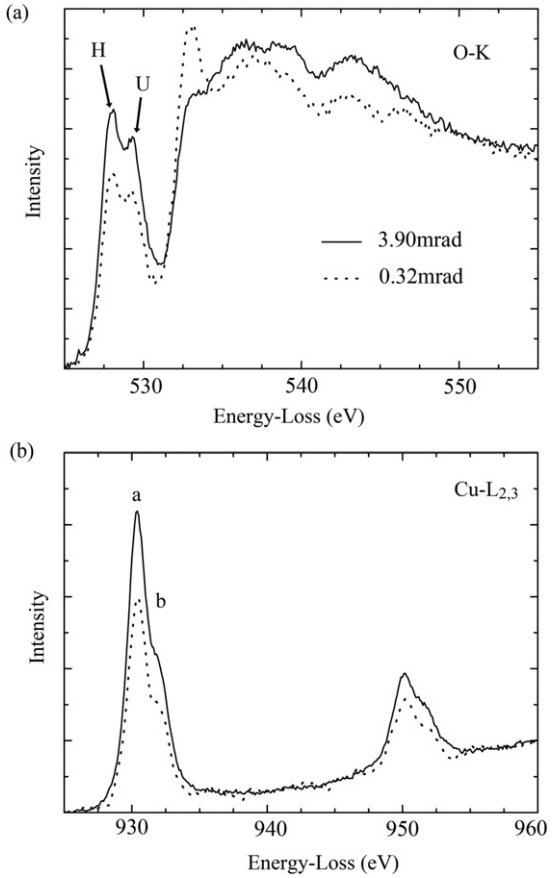

Figure 4. O K (a) and Cu $L_{2,3}$ (b) ionization edges of $Sr_{14}Cu_{24}O_{41}$ recorded in diffraction mode with the incident electron beam parallel to the *b*-axis direction. The collection semi-angles were set to 3.90 mrad (solid) and 0.32 mrad (dot), respectively.

the inelastic scattering for the low-energy loss. We therefore compared the enhanced Cu $L_{2,3}$ edges recorded under electron channeling conditions. The raw experimental spectra were first improved by background subtraction using the power law and then a Fourier ratio deconvolution to remove the plural scattering contribution. The Cu $L_{2,3}$ edges were normalized by the intensity of peak *a* at around 930.5 eV because this peak, corresponding to one intrinsic hole per Cu site, is not sensitive to the O 2p hole states, as discussed above. Figure 5(b) shows the experimental spectra recorded in two different cases, revealing an increase in the intensity of peak *b* in the Cu L_3 line recorded under case II. This intensity rise evidently indicates that there are more holes located in the chains than the ladders. In fact, due to the small difference in the intensity between these two spectra, the difference in the hole density between the two sublattices would be relatively small in comparison with the reported ratio of 6:0 or 5:1 obtained by the optical and XAS measurements [5, 7]. This discrepancy may result from the different methods of the spectra integral, and our result supports the recent one (3.2:2.8) obtained by XAS measurements [6].

Previous structural investigations revealed that substitution of Ca for Sr atoms could result in changes in both incommensurate structural modulation and hole redistribution due to the oxygen atomic displacement [25]. Moreover, the optical

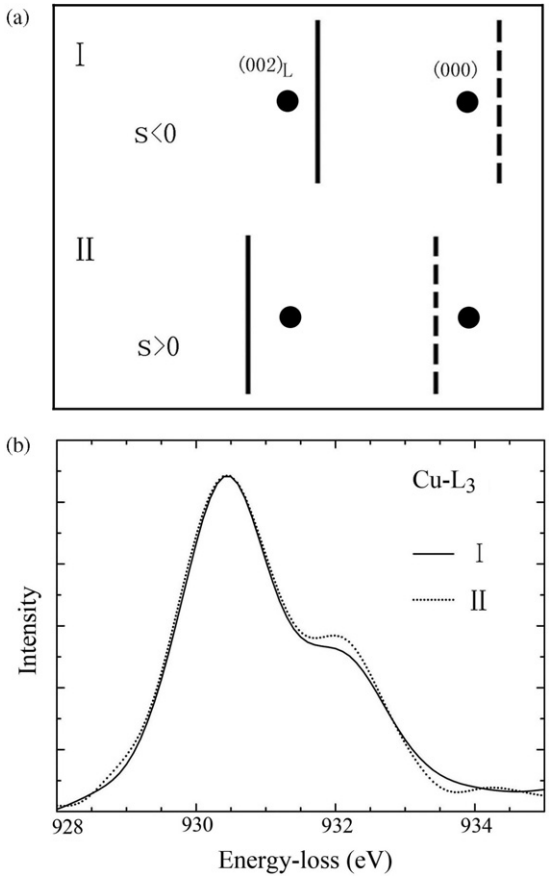

Figure 5. (a) Diffraction geometries used to set up incident-wave intensity with maxima at different sheets. The solid and dashed lines represent the 002 Kikuchi band lines of the ladders. (b) Cu L_3 edges recorded under cases I (solid) and II (dot) as illustrated in (a).

study suggested that holes are transferred from the chains to ladders with Ca substituting for Sr atoms [7]. Figures 6(a) and (b) show respectively the ED patterns taken along the $[1\bar{1}0]$ and [010] zone-axis directions for $Sr_{8.4}Ca_{5.6}Cu_{24}O_{41}$. Compared with $Sr_{14}Cu_{24}O_{41}$, $Sr_{8.4}Ca_{5.6}Cu_{24}O_{41}$ has a similar ED pattern taken along the $[1\bar{1}0]$ zone-axis direction, except for an increase in the intensity of the satellite spots because of the increased intersheet interaction with Ca substitution. On the other hand, the remarkable changes are the positions of the satellite reflections along the c^* direction in the [010] zone-axis ED pattern (figure 6(b)) in which the mesh associated with the chains is largely changed, suggesting that the local structural changes chiefly occur in the chains following oxygen atomic displacements [15]. In addition, the ratio of c_L and c_C estimated from the ED pattern is about 10/7, which is slightly smaller than that of $Sr_{14}Cu_{24}O_{41}$ ($\sim$13/9).

Figures 6(c) and (d) show the typical EEL spectra of the O K- and Cu $L_{2,3}$ edges for the samples at $x = 0$ and 5.6, respectively. These spectra were recorded under the same experimental conditions and agree quite well with the XAS data [5]. It is evident that the spectral weight for the O K edge shows a clear transfer from peak H to U following the substitution of Ca for Sr atoms, and also that peak U shifts slightly towards the high-energy region. As discussed for most cuprates, an increase of formal Cu valence would result in a transfer of spectral weight from the upper Hubbard band U to the hole states H. However, in the present case, the isovalent Ca substitution does not change the total number of holes at all, that is, the average valence of Cu ions remains constant. Hence, it is proposed that the reduction of the spectral weight of U mainly results from charge transfer between the two sublattices and a decrease in hybridization between the O 2p and Cu 3d states, i.e. the increased O 2p character of the hole states. The holes transferred to the ladders would be localized on the O sites. These features can be also recognized by a decrease in the spectral weight of the $Cu^{3+}L_3$ line at about 932.1 eV (figure 6(d)). As a result, the number of nonmagnetic Cu ions would decrease visibly with the Ca substitution, which coincides with the experimental findings for the temperature dependence of the magnetic susceptibility of $Sr_{1-x}Ca_xCu_{24}O_{41}$, in which with increasing Ca concentration, an increase in the magnetic moment evaluated from the susceptibility was observed [26].

In order to further probe hole redistribution between the chains and ladders with substitution of Ca for Sr atoms, we carried out a theoretical simulation of the optical conductivity spectra which are sensitive to the hole density. The hole density dependence of the c-axis optical conductivity spectra, calculated by the DFT + U (5 eV) method for the chains and ladders, is shown in figure 7, in which the changes of the formal Cu valence correspond to the changes of the hole density. The total spectrum, as shown in the inset, agrees well with the experimental one [7, 27]. The low-energy excitations below 1 eV in both sublattices are dominantly contributed by the intraband transitions, and the peaks at 2.1 and 3.0 eV arise from the charge-transfer excitations between the Cu 3d and O 2p states. These charge-transfer excitations are also commonly observed in the parent insulators of the high-T_c superconductors. As a result, according to the theoretical calculations, in the experimental spectra [7], the peak at 2.0 eV is assigned to the excitations in the chains and the peak at 3.0 eV to the summation of the excitations in the chains and ladders, and the low-energy excitations below 1 eV are predominantly contributed by the chains rather than the ladders. With increasing hole density in the ladders, i.e. increasing the valence state of Cu ions, no substantial changes are found in the optical conductivity spectra of the ladders (figure 7(b)). On the other hand, with decreasing hole density in the chains, the peak at 3.0 eV shifts towards the high-energy region and the charge-transfer spectral weight is transferred to the low-energy excitations region below 1.5 eV (figure 7(a)). These features are identical with the Ca substitution dependence of the optical conductivity spectra [7]. Hence, our theoretical results support the argument that holes are transferred from the charge reservoir chains to the ladders with the substitution of Ca for Sr atoms, consistent with the conclusion from our EELS measurements.

Based on the experimental and theoretical results, including the oxygen content dependence of the ratio of c_L and c_C [17], lattice distortion and hole redistribution resulting from substitution of Ca for Sr atoms, it is recognizable that hole distribution between the two sublattices is closely correlated

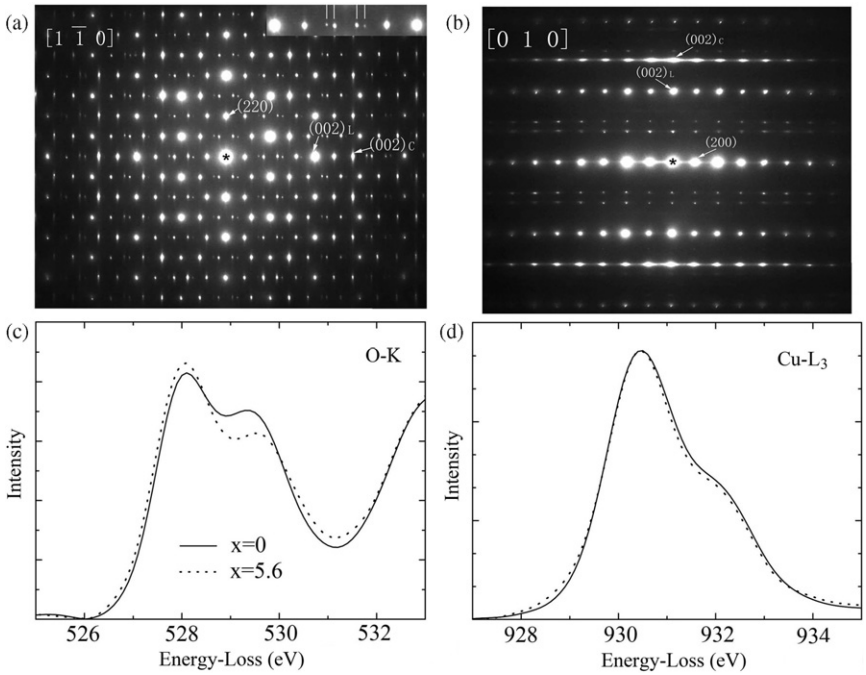

Figure 6. ED patterns of $Sr_{8.4}Ca_{5.6}Cu_{24}O_{41}$ taken along the [1$\bar{1}$0] (a) and [010] (b) zone-axis directions at room temperature. The magnified satellite spots sequence along the c^* direction is shown in the inset. The experimental O K (c) and Cu L_3 (d) ionization edges of $Sr_{14-x}Ca_xCu_{24}O_{41}$ at $x = 0$ (solid) and 5.6 (dot) were recorded under the same conditions.

with the lattice misfit, i.e. the potential given by the lattice modulation [28, 29]. As holes transfer from the chains to ladders, the ratio of c_L and c_C gets smaller, namely, the periodicity corresponding to the superstructure modulation gets larger. Therefore, a typical hole distribution corresponds to the specific periodicity of the modulation arising from the lattice misfit between the two sublattices, and this kind of structural modulation is not affected by the charge localization in the chains at low temperature.

As mentioned above, the notable feature in the present system is the lattice misfit along the c-axis direction, which induces modulated structural features in both the chains and the ladders. This modulation generates a pinning potential which determines the chief features of the charge ordered state [18]. As shown in the ED patterns, the satellite spots can be uniquely indexed using multiple diffraction due to the two interpenetrating structures. Upon cooling the sample to 20 K, no additional superstructure appears, and no temperature dependence can be observed in the positions of these satellite spots. On the other hand, it is noted that the superlattice given by the lattice misfit at room temperature basically agrees with that observed in x-ray and neutron diffraction experiments in which the superstructure is considered to arise from the charge ordering. For instance, the wavevector of the ladder modulation, $q = (0, 0, 0.2)_L$ or $(0, 0, 0.25)_L$ reported in [11, 29, 30], corresponds to wavevector $q = (0, 0, 0.228)_L$ in our ED experiments, and the wavevector of the chain modulation, $q = (0, 0, 0.318)_C$ [31] or $(0, 0, 1/3)_C$ [32], corresponds to wavevector $q = (0, 0, 0.311)_C$. The discrepancy in the modulated periodicities obtained by different measurements possibly results from different oxygen or doping concentration of the samples used in the experiments, because the specific hole distribution as well as lattice misfit depends on the oxygen and doping concentration. Therefore, the additional modulation reflections, observed in x-ray and neutron diffraction experiments at low temperature, can be described as the higher-order reflections of the incommensurate modulation occurring at room temperature which exhibit pronounced temperature dependence in intensity, as discussed by Zimmermann *et al* [18]. Moreover, it is also possible that the periodicity arising from the charge ordering at low temperature has the same value as that of the superlattice given by the lattice misfit, suggesting that the charge ordering and magnetic transition do not introduce any additional superstructures in the present system at low temperature. Therefore, it would be impossible to detect such a superstructure generated by the charge ordering in the ED experiments.

4. Summary

In summary, using electronic structure calculations, TEM observations and EELS measurements, we examined the crystal structure and electronic structure of the spin-ladder compound $Sr_{14-x}Ca_xCu_{24}O_{41}$ and accounted for the relationship between the structural modulation and electronic structure. The incommensurate modulation goes along the c-axis direction due to the lattice misfit between the two sublattices. The temperature independence of the positions of the satellite spots indicates that no additional superstructure emerges at low temperature. Substitution of Ca for Sr atoms in $Sr_{14-x}Ca_xCu_{24}O_{41}$ reduces the ratio of c_L and c_C and yields clear changes in the structural modulation. According

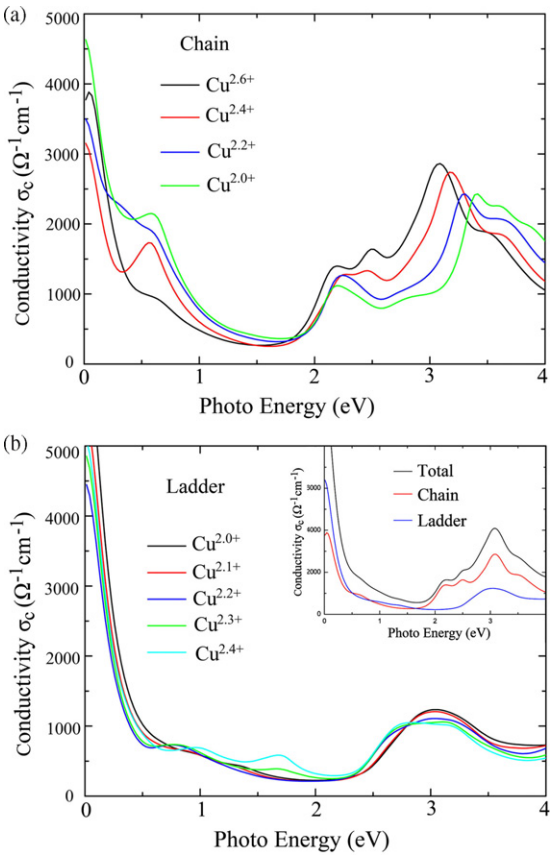

Figure 7. Hole density dependence of the *c*-axis optical conductivity spectra for the chain (a) and ladder (b) sublattices calculated by the DFT + U method. The total spectrum with all six holes located in the chains is shown in the inset. See the text for details.

to the electron channeling effect, the selectively enhanced spectra for each sublattice indicate that the hole density in the chains is larger than that in the ladders. Moreover, the experimental EELS measurements in combination with the theoretical simulation of optical conductivity spectra show that holes are transferred from the chains to the ladders following the substitution of Ca for Sr atoms. Based on our experimental and theoretical results, it is evident that both the structural modulation and the hole distribution between the chains and ladders are closely related to the lattice misfit; this fact explains why different lattice misfits are observed in compounds with different Ca doping or oxygen content.

Acknowledgments

This work is supported by the National Science Foundation of China (No. O7J1091A61 and 10674105), the Knowledge Innovation Project of the Chinese Academy of Sciences, and the 973 project of the Ministry of Science and Technology of China.

References

[1] Dagotto E, Riera J and Scalapino D 1992 *Phys. Rev.* B **45** 5744
[2] Dagotto E and Rice T M 1996 *Science* **271** 618
[3] Uehara M, Nagata T, Akimitsu J, Takahashi H, Môri N and Kinoshita K 1996 *J. Phys. Soc. Japan* **65** 2764
[4] McCarron E M, Subramanian M A, Calabrese J C and Harlow R L 1988 *Mater. Res. Bull.* **23** 1355
[5] Nücker N, Merz M, Kuntscher C A, Gerhold S, Schuppler S, Neudert R, Golden M S, Fink J, Schild D, Stadler S, Chakarian V, Freeland J, Idzerda Y U, Conder K, Uehara M, Nagata T, Goto J, Akimitsu J, Motoyama N, Eisaki H, Uchida S, Ammerahl U and Revcolevschi A 2000 *Phys. Rev.* B **62** 14384
[6] Rusydi A, Berciu M, Abbamonte P, Smadici S, Eisaki H, Fujimaki Y, Uchida S, Rubhausen M and Sawatzky G A 2007 *Phys. Rev.* B **75** 104510
[7] Osafune T, Motoyama N, Eisaki H and Uchida S 1997 *Phys. Rev. Lett.* **78** 1980
[8] Abbamonte P, Blumberg G, Rusydi A, Gozar A, Evans P G, Siegrist T, Venema L, Eisaki H, Isaacs E D and Sawatzky G A 2004 *Nature* **431** 1078
[9] Zhang F C and Rice T M 1998 *Phys. Rev.* B **37** 3759
[10] Carter S A, Batlogg B, Cava R J, Krajewski J J, Peck W F Jr and Rice T M 1996 *Phys. Rev. Lett.* **77** 1378
[11] Fukuda T, Mizuki J and Matsuda M 2002 *Phys. Rev.* B **66** 012104
[12] Zeng Y, Shi J, Yu Z and Pan F 2005 *Mater. Lett.* **59** 662
[13] Egerton R F 1996 *Electron Energy-Loss Spectroscopy in the Electron Microscope* 2nd edn (New York: Plenum)
[14] Blaha P, Schwarz K, Madsen G, Kvasnicka D and Luitz J 2001 *WIEN2K, An Augmented Plane Wave + Local Orbital Program for Calculating Crystal Properties* Wien, Austria Karlheinz Schwarz, Technical University
[15] Etrillard J, Braden M, Gukasov A, Ammerahl U and Revcolevschi A 2004 *Physica* C **403** 290
[16] Wang J, Zou H, Guo C, Wang L, Hu N and Shi J 2007 *J. Phys.: Condens. Matter* **19** 196224
[17] Hiroi Z, Amelinckx S, Van Tendeloo G and Kobayashi N 1996 *Phys. Rev.* B **54** 15849
[18] Zimmermann M V, Geck J, Kiele S, Klingeler R and Büchner B 2006 *Phys. Rev.* B **73** 115121
[19] Schwingenschlogl U and Schuster C 2007 *Eur. Phys. J.* B **55** 43
[20] Arai M and Tsunetsugu H 1997 *Phys. Rev.* B **56** R4305
[21] Fink J, Nücker N, Pellegrin E, Romberg H, Alexander M and Knupfer M 1994 *J. Electron Spectrosc. Relat. Phenom.* **66** 395
[22] Zaanen J, Sawatzky G A and Allen J W 1985 *Phys. Rev. Lett.* **55** 418
[23] Tafto J and Krivanek O L 1982 *Phys. Rev. Lett.* **48** 560
[24] Tatsumi K, Muto S, Yamamoto Y, Ikeno H, Yoshioka S and Tanaka I 2006 *Ultramicroscopy* **106** 1019
[25] Gotoh Y, Yamaguchi I, Takahashi Y, Akimoto J, Goto M, Onoda M, Fujino H, Nagata T and Akimitsu J 2003 *Phys. Rev.* B **68** 224108
[26] Motoyama N, Osafune T, Kakeshita T, Eisaki H and Uchida S 1997 *Phys. Rev.* B **55** R3386
[27] Popovic Z V, Konstantinovic M J, Ivanov V A, Khuong O P, Gajic R, Vietkin A and Moshchalkov V V 2000 *Phys. Rev.* B **62** 4963
[28] Gelle A and Lepetit M-B 2004 *Phys. Rev. Lett.* **92** 236402
[29] Braden M, Etrillard J, Gukasov A, Ammerahl U and Revcolevschi A 2004 *Phys. Rev.* B **69** 214426
[30] Cox D E, Iglesias T, Hirota K, Shirane G, Matsuda M, Motoyama N, Eisaki H and Uchida S 1998 *Phys. Rev.* B **57** 10750
[31] Rusydi A, Abbamonte P, Eisaki H, Fujimaki Y, Blumberg G, Uchida S and Sawatzky G A 2006 *Phys. Rev. Lett.* **97** 016403
[32] Rusydi A, Abbamonte P, Eisaki H, Fujimaki Y, Smadici S, Motoyama N, Uchida S, Kim Y-J, Rubhausen M and Sawatzky G A 2008 *Phys. Rev. Lett.* **100** 036403